Iroquois homeobox gene 3 establishes fast conduction in the cardiac His–Purkinje network

Shan-Shan Zhang[a,b,c,d,1], Kyoung-Han Kim[e,f,g,1], Anna Rosen[e,f,g,1], James W. Smyth[h,i,1], Rui Sakuma[c,1], Paul Delgado-Olguín[a], Mark Davis[e], Neil C. Chi[h,i,j,2], Vijitha Puviindran[c], Nathalie Gaborit[a], Tatyana Sukonnik[a], John N. Wylie[a], Koroboshka Brand-Arzamendi[h,j], Gerrie P. Farman[e], Jieun Kim[c,d], Robert A. Rose[e,f,3], Phillip A. Marsden[g], Yonghong Zhu[c], Yu-Qing Zhou[k], Lucile Miquerol[l], R. Mark Henkelman[k,m], Didier Y. R. Stainier[h,j], Robin M. Shaw[h,i], Chi-chung Hui[c,d,4], Benoit G. Bruneau[a,b,h,n,4], and Peter H. Backx[e,f,g]

[a]Gladstone Institute of Cardiovascular Disease, San Francisco, CA 94158; [b]Program in Biomedical Science, [h]Cardiovascular Research Institute, and Departments of [i]Medicine, [j]Biochemistry and Biophysics, and [n]Pediatrics, University of California, San Francisco, CA 94143; [c]Program in Developmental and Stem Cell Biology, Hospital for Sick Children, Toronto, ON, Canada M5G 1X8; Departments of [d]Molecular Genetics, [f]Medicine, [g]Physiology, and [m]Medical Biophysics and [e]Division of Cardiology at University Health Network University of Toronto, Toronto, ON, Canada M5S 3E2; [k]Mouse Imaging Centre, Toronto, ON, Canada M5G 1X8; and [l]Institut de Biologie du Développement de Marseille-Luminy, 13288 Marseille Cedex 9, France

Edited by Jonathan G. Seidman, Harvard Medical School, Boston, MA, and approved July 5, 2011 (received for review May 2, 2011)

Rapid electrical conduction in the His–Purkinje system tightly controls spatiotemporal activation of the ventricles. Although recent work has shed much light on the regulation of early specification and morphogenesis of the His–Purkinje system, less is known about how transcriptional regulation establishes impulse conduction properties of the constituent cells. Here we show that *Iroquois homeobox gene 3* (*Irx3*) is critical for efficient conduction in this specialized tissue by antithetically regulating two gap junction–forming connexins (Cxs). Loss of *Irx3* resulted in disruption of the rapid coordinated spread of ventricular excitation, reduced levels of Cx40, and ectopic Cx43 expression in the proximal bundle branches. Irx3 directly represses Cx43 transcription and indirectly activates Cx40 transcription. Our results reveal a critical role for Irx3 in the precise regulation of intercellular gap junction coupling and impulse propagation in the heart.

development | electrophysiology | transcription factor

With each heartbeat, electrical impulses generated by the sinoatrial node travel through the atria, pause at the atrioventricular node, and proceed to the ventricular conduction system (VCS), also known as the His–Purkinje network. Rapid impulse conduction in the VCS tightly controls the spatiotemporal mechanical activation of the ventricles, thereby optimizing pump function (1). Conduction through the VCS is impaired in several inherited forms of cardiac conduction disorders and is associated with increased risk of arrhythmias and heart disease (2). At the cellular level, efficient impulse propagation through this network is dependent upon the interplay between cell morphology, membrane excitability, and electrical coupling of adjacent cells via gap junctions, the latter of which is the major determinant for rapid and directional conduction (3). Although regulation of early VCS specification and morphogenesis is becoming well understood (4–9), less is known about how cells of the VCS gain their specialized conduction properties as they mature.

The *Iroquois homeobox* (*Irx*) gene family of transcription factors contains a highly conserved DNA-binding homeodomain of the 3-amino acid loop extension superclass and is characterized by an 11-amino acid *Iro* motif. *Irx* genes have evolutionarily conserved roles during embryonic development (10) and can act as either repressors or activators of gene expression depending on the cellular context (11–13). All six *Irx* genes are expressed in partially overlapping patterns in the developing mouse heart (12–16). The functional significance of *Irx3* in the heart remains unknown.

Results and Discussion

We examined the developmental expression of *Irx3* in mice in which sequences encoding the *tauLacZ* fusion protein (17) were inserted at the translational start site to create a loss-of-function reporter allele ($Irx3^{tauLacZ}$; Fig. S1*A*). The *tauLacZ* reporter recapitulated endogenous *Irx3* mRNA expression in the central nervous system of the developing embryo (Fig. 1*A*; ref. 14). At embryonic day (E) 10, a ring-like group of $Irx3^{tauLacZ+}$ cells was detected in the developing ventricle. Analysis of E11 heart sections revealed that these cells represent a subset of developing trabeculae and cells surrounding the emerging interventricular septum (IVS), which are thought to contribute to the VCS (ref. 18; Fig. 1*B*). From E14 onwards, $Irx3^{tauLacZ}$ was expressed in cells of the bifurcating His bundle primordium atop the IVS, subendocardial bundle branches along the septum, and trabeculae (ref. 18; Fig. 1 *C* and *F* and Movie S1).

The adult VCS is highly asymmetric and comprises the bundle of His, subendocardial bundle branches, and Purkinje fibers (19). Cells expressing $Irx3^{tauLacZ}$ matured into a highly elaborate network during postnatal maturation, marking the common His bundle, which branched into a fan-like group of smaller bundles along the left septal flank (Fig. 1*G* and Fig. S2 *A* and *C*). In contrast, only a few thin bundles branched away from the common bundle on the right side of the heart (Fig. 1 *D* and *G*, Fig. S2*B*, and Movie S2). These subendocardial bundles extended further toward the apex to form a dense network of interlaced fascicles connecting the free wall and septum (Fig. 1*D*). *Irx3* was expressed in the His bundle, which was ensheathed in a fibrous matrix in adult hearts (Fig. 1*E*).

At E14.5, $Irx3^{tauLacZ+}$ cells were surrounded by endocardial cells marked by platelet/endothelial cell adhesion molecule-1 (PECAM) and expressed the muscle-specific actin-binding protein tropomyosin (Fig. S2 *D* and *E*). These subendocardial $Irx3^{+}$ myocytes coexpressed established markers of the conduction sys-

Author contributions: S.-S.Z., K.-H.K., A.R., J.W.S., R.S., N.C.C., R.M.S., C.-c.H., B.G.B., and P.H.B. designed research; S.-S.Z., K.-H.K., A.R., J.W.S., R.S., P.D.-O., M.D., N.C.C., V.P., N.G., T.S., J.N.W., K.B.-A., G.P.F., J.K., R.A.R., Y.Z., and Y.-Q.Z. performed research; P.A.M. and L.M. contributed new reagents/analytic tools; S.-S.Z., K.-H.K., A.R., J.W.S., P.D.-O., N.C.C., N.G., R.A.R., Y.-Q.Z., R.M.H., D.Y.R.S., R.M.S., C.-c.H., B.G.B., and P.H.B. analyzed data; and S.-S.Z., K.-H.K., A.R., J.W.S., C.-c.H., B.G.B., and P.H.B. wrote the paper.

The authors declare no conflict of interest.

This article is a PNAS Direct Submission.

Freely available online through the PNAS open access option.

[1]S.-S.Z., K.-H.K., A.R., J.W.S., and R.S. contributed equally to this work.

[2]Present address: University of California at San Diego, La Jolla, CA 92093.

[3]Present address: Department of Physiology and Biophysics, Faculty of Medicine, Dalhousie University, Halifax, NS, Canada B3H 4R2.

[4]To whom correspondence may be addressed. E-mail: bbruneau@gladstone.ucsf.edu or cchui@sickkids.ca.

This article contains supporting information online at www.pnas.org/lookup/suppl/doi:10.1073/pnas.1106911108/-/DCSupplemental.

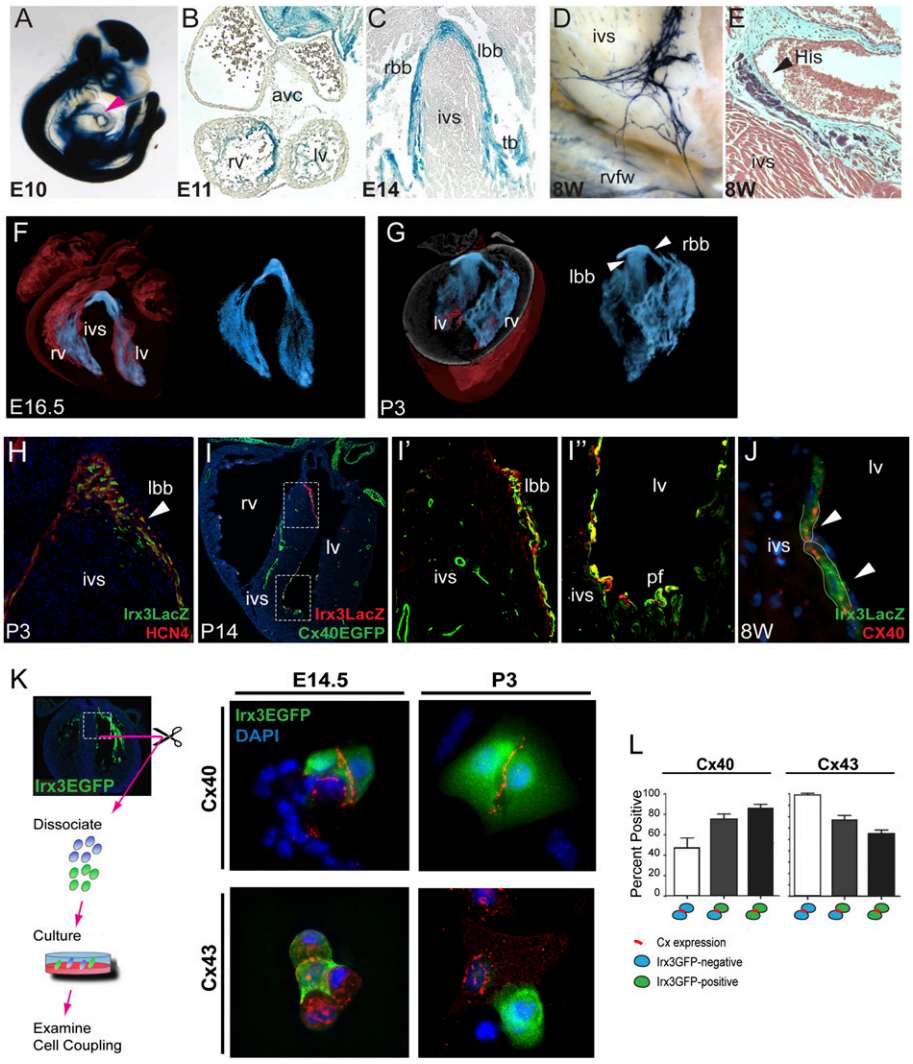

Fig. 1. *Irx3* is highly expressed in the developing and mature His–Purkinje network. (*A–D*) β-Galactosidase staining of $Irx3^{tauLacZ/+}$ embryos at E10 (*A*), E11 (*B*), E14 (*C*), and in adult heart (*D*). Arrowhead in *A* shows a ring-like group of cells that is detected in the developing ventricle. (*E*) Masson's trichrome staining reveals fibrous insulation of the $Irx3^{tauLacZ+}$ bundle of His in an adult heart. (*F* and *G*) Optical projection tomography (OPT) images of $Irx3^{tauLacZ}$ expression at E16.5 (*F*) and postnatal day 3 (P3; *G*). (*H*) Immunofluorescence colocalization of $Irx3^{tauLacZ}$ and Hcn4 in the VCS at P3. (*I*) Colocalization of $Irx3^{tauLacZ}$ and $Cx40^{EGFP}$ in the VCS of $Irx3^{tauLacZ/+}$; $Cx40^{EGFP/+}$ mice at P14, including bundle branches (*I'*) and Purkinje fibers (*I''*). (*J*) Adult $Irx3^{tauLacZ+}$ bundle branch cells express Cx40 at longitudinal cell borders. (*K*) Immunostaining of reaggregated cells for Cx40, Cx43, and EGFP E14.5 and P3. (*L*) Quantitation of gap junctions formed between reaggregated cells. avc, atrioventricular canal; rv, right ventricle; lv, left ventricle; rbb, right bundle branch; lbb, left bundle branch; tb, trabeculae; rvfw, right ventricular free wall; His, bundle of His.

tem such as hyperpolarization-gated cyclic nucleotide-gated family potassium channel 4 (Hcn4),and connexin 40 (Cx40; also known as gap junction alpha-5 protein, or Gja5) (Fig. 1 *H–J* and Fig. S2*F*). In 8-wk-old adult mice, cells with high levels of $Irx3^{tauLacZ}$ expressed Cx40 protein at longitudinal ends of the cell (Fig. 1*J*). $Irx3^{tauLacZ+}$ cells, with the exception of those marking the distal VCS in the left ventricle, were predominantly derived from the *Mef2CAHF::Cre*-labeled ventricular myocyte lineage (ref. 20; Fig. S2*H*). Moreover, $Irx3^{tauLacZ+}$ VCS cells were not derived from the *Wnt1–Cre*-labeled neural crest lineage (ref. 21; Fig. S2*G*). Together, these findings demonstrate that *Irx3* expression is highly enriched in the specialized myocytes of the VCS, arising from a *Mef2CAHF::Cre*-expressing ventricular lineage.

We sought to determine whether cells expressing Irx3 exhibit connexin (Cx) expression patterns characteristic of VCS myocytes. Fluorescence from *Irx3::EGFP BAC* transgenic reporter mice (Fig. S3) was used to identify *Irx3*-expressing myocytes isolated from the proximal VCS. In agreement with the gradual enrichment of Cx40 to VCS and down-regulation of Cx43 in these cells during development (22), quantitation of Cx plaque expression between cell pairs showed that the majority of cells from the proximal VCS ($Irx3::EGFP^{+}$) expressed Cx40 between cells (Fig. 1 *K* and *L*). In contrast, Cx43 plaques were mostly enriched in non-$Irx3::EGFP^{+}$ cells. These specific properties of *Irx3*-expressing cells are consistent with those of conduction myocytes of the VCS.

We then examined the phenotype of $Irx3^{taulacZ/tauLacZ}$ mice to assess *Irx3* function. *Irx3*-null mice were viable and fertile and did not manifest abnormalities in heart morphology, heart-to-body size ratio, or contractile function assessed by echocardiography (Dataset S1). However, by 2 wk of age, they exhibited ventricular activation defects when assessed by surface electrocardiography (ECG). These mice exhibited prolonged QRS and notched R waves (R'), both indicative of delays in ventricular activation (Fig. 2 *A* and *B* and Fig. S4*A*). These ECG defects were also observed in freely moving mice by telemetry ECG and in ex vivo perfused hearts (Fig. 2*B* and Fig. S4*C*). Right axis deviation, detected as a negative QRS deflection in lead I combined with a positive deflection in lead II, was observed in 70% of *Irx3*-null mice (Fig. 2*A*). These observations suggest bundle branch block or abnormal impulse conduction, perhaps in the right ventricular free wall, as underlying mechanisms of the observed abnormal ventricular activation phenotype. In the absence of abnormal heart orientation or structural changes, these data point to a conduction defect in the VCS (23), where Irx3 is normally highly expressed. Indeed, intracardiac ECG recordings revealed that, although impulse spread from the atria to the His bundle (AH interval) was unaffected by the loss of *Irx3*, there was an increase of the conduction time between the His bundle and ventricles (HV interval; Fig. 2 *C* and *D* and Fig. S4*B*).

Optical mapping of epicardial activation confirmed abnormal activation of the ventricles (Fig. 2*E*). Indeed, in wild-type mice,

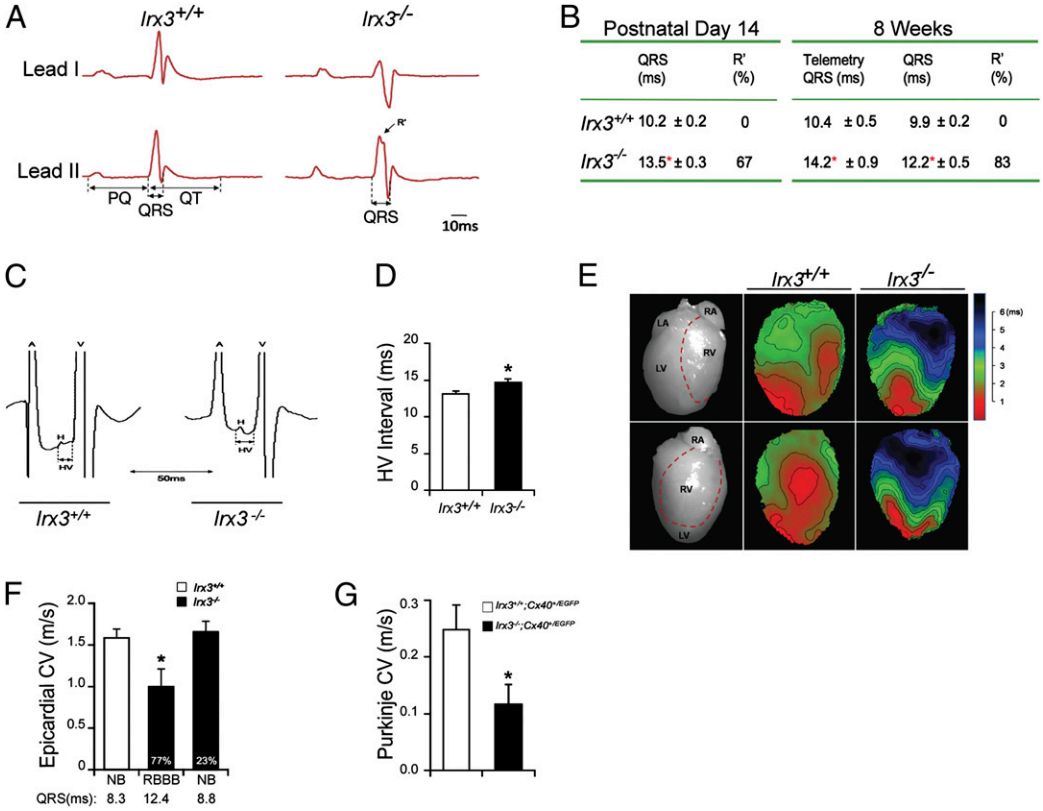

Fig. 2. *Irx3* is required for normal ventricular activation. (*A*) Representative six-lead surface ECG tracing shows prolongation of the QRS and abnormal R′ wave in *Irx3*-null mice. (*B*) A summary of six-lead and telemetry ECG parameters. $n = 8–12$; $^*P < 0.05$ vs. wild type. (*C*) Representative octapolar intracardiac ECG traces illustrating atrial, ventricular, and His-bundle depolarization signals. (*D*) Quantification of HV prolongation. $n = 9$; $^*P < 0.05$. (*E*) Optical mapping results shown in apical four-chamber view and apical right ventricular two-chamber view. Isochrone lines mark areas where depolarization reached 50% intensity in consecutive 0.5-ms intervals. Depolarization proceeds in an apex-to-base direction. Red indicates earliest activation time (ms). Wild type, $n = 12$; *Irx3*-null, $n = 9$. (*F*) Quantitation of epicardial conduction velocity (CV) and corresponding QRS. We found that 77% of hearts lacking Irx3 had RBBB, slowed epicardial CV, and QRS widening, in comparison with wild-type hearts, and that 23% of *Irx3*-null hearts that did not show conduction block (NB). Values are mean ± SEM; $n = 4–6$; $^*P < 0.05$. (*G*) Quantitation of VCS fiber CV in $Irx3^{tauLacZ/tauLacZ};Cx40^{EGFP/+}$ fibers compared with $Irx3^{+/+};Cx40^{EGFP/+}$ mice. Values are means ± SEM; $n = 6–7$; $^*P < 0.05$.

activation was characterized by simultaneous "breakthrough" depolarization of both ventricles, presumably via the right and left bundle branches (24), whereas the majority (77%) of *Irx3*-null hearts had a single breakthrough from the left ventricular apex, along with significantly slowed conduction velocity (Fig. 2*F*). These findings establish that the abnormal ventricular activation phenotype in the *Irx3*-null mice is characterized by right bundle branch block (RBBB). Restriction of the defective conduction to the right bundle, despite the absence of Irx3 in the entire VCS of *Irx3*-null mice, can be explained by the lower safety factor for conduction in right conduction pathway (25, 26), where constituent cells form only 1 or 2 bundles and have shorter action potential durations (19, 27) compared with the large group of bundles in the left pathway (~20 bundles). To examine whether RBBB is caused by conduction slowing or by complete block, conduction velocity was measured in the VCS of mice expressing the $Cx40^{EGFP}$ reporter. $Irx3^{taulacZ/taulacZ};Cx40^{EGFP/+}$ mice had significantly diminished conduction velocity through the conduction fibers compared with $Cx40^{EGFP/+}$ mice (Fig. 2*G*). These results show that observed abnormal ventricular activation is due to conduction slowing in cells lacking Irx3.

Given that electrical coupling of adjacent cells is a major determinant for rapid and directional conduction, we examined the expression level and composition of gap junctions, which dictate cell–cell coupling efficiency and ensure orchestrated current flow (3). The specific expression pattern of Cxs comprising the VCS gap junctions is thought to ensure appropriate coupling within this tissue compartment, while ensuring functional insulation from the working myocardium (28). We examined Cx protein expression in the heart and found that Cx40, which is normally highly expressed throughout the VCS, was reduced in hearts lacking *Irx3* (Fig. 3 *A* and *B* and Fig. S5 *A* and *B*). Using laser capture microdissection (LCM), we found that Cx40 (*Gja5*) mRNA was lower in the Purkinje fibers of $Irx3^{tauLacZ/tauLacZ};Cx40^{EGFP/+}$ mice compared with $Cx40^{EGFP/+}$ littermates, revealing less than expected gene expression from the remaining Cx40 allele (Fig. 3*C* and Fig. S5 *C–I*).

However, lower Cx40 expression may not fully account for the ventricular activation phenotype because hearts from $Cx40^{EGFP/+}$ mice show normal activation (refs. 29–31; Fig. S4*D*), despite having reduced Cx40 expression that is similar to that found in the *Irx3*-null mice. Consistent with this conjecture, we detected ectopic Cx43 expression in the proximal bundle branches, marked by *Irx3::EGFP*, where only nominal expression of Cx43 normally occurs at P5 (Fig. 3 *D* and *E*). At the adult stage, high-resolution immunofluorescence imaging revealed ectopic Cx43 expression at cell borders between $Irx3::EGFP^+$ VCS myocytes and between non-GFP working myocytes and $Irx3::EGFP^+$ VCS myocytes in hearts lacking Irx3 (Fig. 3 *F* and *G* and Fig. S5*J*). Cell pairs from reaggregated neonatal myocytes isolated from the proximal VCS were analyzed for clear Cx43 plaque expression at cell–cell borders marked by N-cadherin. In the absence of

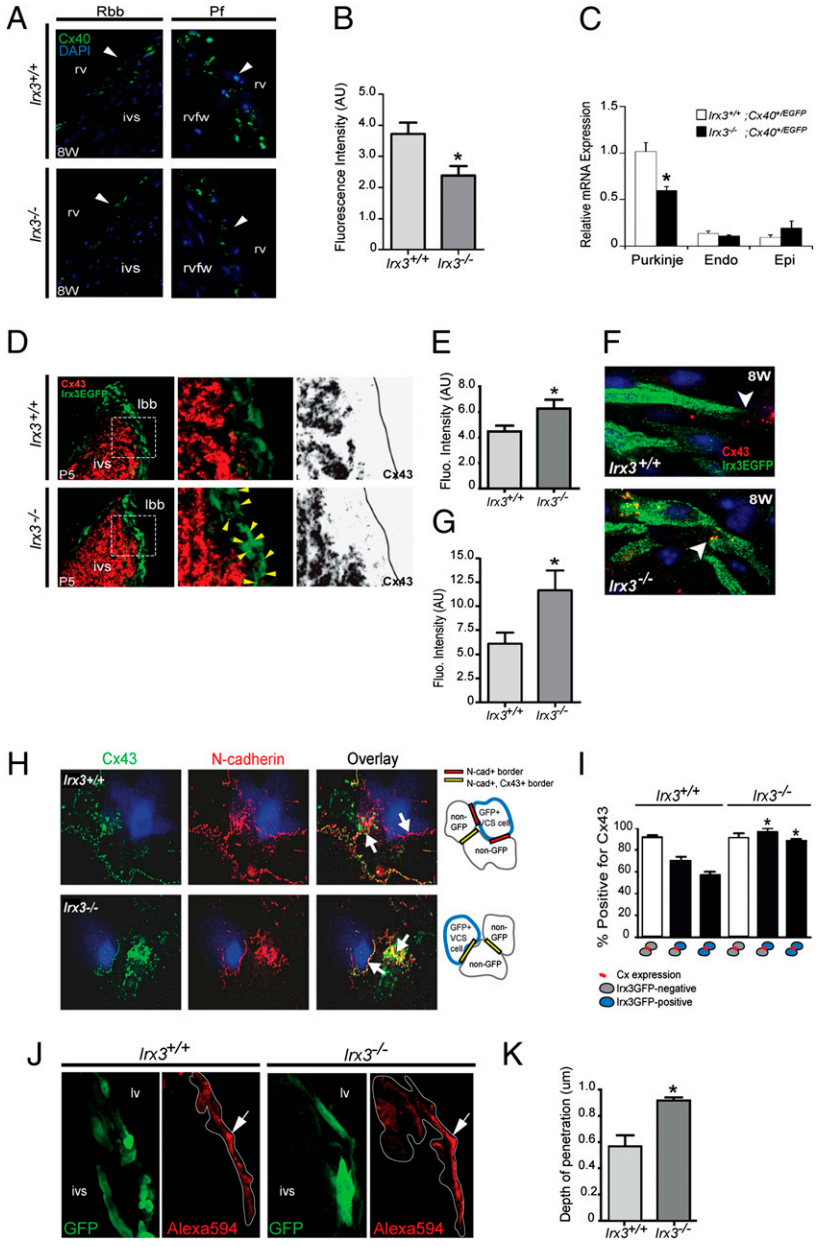

Fig. 3. *Irx3* regulates Cx40 and Cx43 expression in the VCS. (*A*) Representative Cx40 immunofluorescence images of the right bundle branch and right ventricular free wall Purkinje fibers of wild-type (WT) and *Irx3*-null mice at 8 wk. (*B*) Quantitation of Cx40$^+$ plaques. (*C*) qRT-PCR analysis of LCM captured adult VCS cells for *Gja5* mRNA in $Irx3^{tauLacZ/tauLacZ}$;$Cx40^{EGFP/+}$ vs. $Irx3^{+/+}$;$Cx40^{EGFP/+}$ hearts. (*D*) Representative Cx43 immunofluorescence images. Arrowheads show ectopic Cx43$^+$ plaques in *Irx3::EGFP*$^+$ proximal bundle branch cells of *Irx3*-null mice at P5. Grayscale images show intensity mask for Cx43 signal. (*E*) Plaque intensity was quantified by using ImageJ software. *$P < 0.05$ vs. WT. (*F*) Adult heart confocal imaging at 100× magnification shows ectopic Cx43$^+$ plaques at conduction-working myocyte and conduction–conduction myocyte borders in the absence of Irx3. (*G*) Plaque intensity was quantified by using ImageJ software. *$P < 0.05$ vs. WT. (*H*) Immunofluorescence for Cx43 (green), N-cadherin (red), and EGFP (blue) of cells reaggregated from the VCS of either WT or *Irx3*-null mice, each expressing the *Irx3::EGFP* reporter. (*I*) Quantitation of Cx43 plaque expression at cell–cell borders. $n = 80$; *$P < 0.05$ vs. WT. (*J* and *K*) Fluorescent dye spread (white outline) in microinjected proximal right bundle branch cells (marked by *Irx3::EGFP*$^+$). *$P < 0.05$ vs. WT. rvfw, right ventricular free wall; Pf, Purkinje fibers; LBB, left bundle branch; Endo, endocardium; Epi, epicardium.

Irx3, a higher number of cell borders between VCS cells (marked by *Irx3::EGFP*) and non-GFP$^+$ working myocytes contained Cx43$^+$ plaques compared with wild type (Fig. 3 *H* and *I*). The presence of Cx43 in the VCS may cause slowing of impulses through the formation of heterotypic Cx40–Cx43 gap junctions that cannot conduct impulses efficiently (32) or may be due to ectopic gap junctions coupling the VCS to the working myocardium, resulting in lateral spread of excitation.

To better understand how the observed changes in Cx expression could underlie conduction slowing, we used a dye-coupling assay (33) in which the spread of Alexa 594 from microinjected cells of the proximal right bundle branches was measured to examine intercellular communication. Dye spread was predominantly restricted within *Irx3::EGFP*$^+$ VCS cells in wild-type hearts, whereas hearts lacking Irx3 displayed significantly higher depth of dye spread from bundle branch cells to the non-GFP working myocardium (Fig. 3 *J* and *K*). These data, combined with our immunofluorescence results, demonstrate that ectopic Cx43 in the proximal conducting system allows abnormal communication between VCS cells and the working myocardium. Presumably, Cx43 expression in the myocytes of the proximal VCS allows functional gap junctions to form with the working myocardium via Cx43–Cx43 hemichannels (34–36). This abnormal coupling is expected to cause impulse dispersion away from the conduction axis, as well as to promote conduction block through charge dissipation from the smaller VCS source to the large ventricular sink.

To gain mechanistic insight into the molecular basis for the antithetic regulation of Cx40 and Cx43 by *Irx3*, we examined Cx40 (*Gja5*) and Cx43 (*Gja1*) expression in isolated neonatal ventricular myocytes (NVMs) infected with adenovirus encoding GFP, Irx3, dominant Irx3 activator (*VP16–Irx3*), or dominant Irx3 repressor (*EnR–Irx3*; Fig. 4*A*). Infected NVMs overexpressed comparable levels of Irx3 mRNA and protein (Fig. S6 *A* and *B*). Consistent with the observed Cx40 decrease in the VCS of *Irx3*-null mice, Cx40 protein and mRNA were increased by Irx3 overexpression in NVMs (Fig. 4 *B* and *C*). Interestingly, *EnR–Irx3* overexpression promoted *Gja5* expression, whereas *VP16–*

DEVELOPMENTAL BIOLOGY

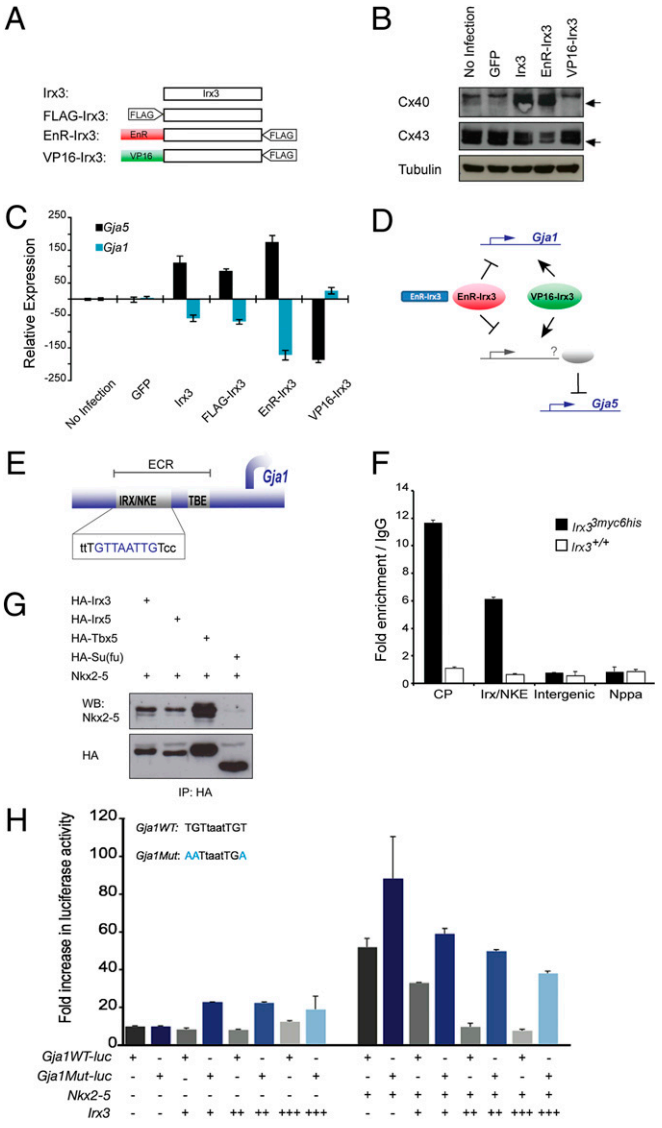

Fig. 4. Transcriptional regulation of *Cx40* and *Cx43* gene expression by *Irx3*. (*A*) NVMs were infected with the following adenoviral constructs: GFP control (*Ad-GFP*), Irx3 (*Ad-Irx3*, *Ad-FLAG-Irx3*), Irx3 fused to the VP16 activation domain (*Ad-VP16-Irx3*), or the Engrailed suppressor domain (*Ad-EnR-Irx3*). (*B*) Cx40 and Cx43 protein expression. (*C*) Quantitation of *Gja1* and *Gja5* mRNA compared with noninfected and GFP-infected cells. (*D*) Schematic depicting regulation of *Gja1* and *Gja5* transcription by dominant active and dominant negative forms of Irx3 in infected NVMs. (*E*) Genome alignment analysis of the *Gja1* promoter revealed an evolutionarily conserved element containing a putative *Irx3* binding site that overlaps with an Nkx2-5 binding motif (Irx/NKE), immediately upstream of T-box binding elements (TBE). (*F*) Chromatin immunoprecipitation using ventricles from $Irx3^{3myc\text{-}6his}$ mice shows enrichment of *Irx3* at the conserved Irx/NKE site and core promoter, but not at an intergenic region or the *Nppa* promoter. (*G*) Coimmunoprecipitation of Irx3 with Nkx2-5 and Tbx5. Su(fu) serves as negative control. (*H*) Luciferase activity of *Gja1–luciferase* in cells cotransfected with *Irx3* or *Nkx2-5* expression constructs. *Gja1mut* indicates a *Gja1–luciferase* reporter in which three point mutations were made in the evolutionarily conserved core binding sequence. ECR, evolutionarily conserved region; CP, core promoter; Irx/NKE, evolutionarily conserved binding site for Irx3 and Nkx2-5.

Irx3 inhibited *Gja5* expression. This result suggests that Irx3 likely regulates *Gja5* indirectly, activating *Gja5* expression by suppressing the transcription of a *Gja5* repressor. In contrast, our results indicate that Irx3 directly represses *Gja1* transcription. In agreement with a repressive role of Irx3 on Cx43 expression in vivo, Cx43 protein and mRNA (Fig. 4 *B* and *C* and Fig. S6 *C* and *D*) were reduced in cells overexpressing Irx3. Furthermore, *Gja1* mRNA was markedly decreased in the presence of *EnR–Irx3* but increased slightly in response to *VP16–Irx3*. The effects of dominant repressor and activator forms of Irx3 on the Cx promoters is summarized in Fig. 4*D*. Given that *Iroquois* proteins commonly act as transcriptional repressors, our data support antithetical regulation of Cx40 and Cx43 expression by *Irx3* through direct as well as indirect mechanisms.

Promoter analysis of Cxs that are expressed in the VCS (Cx40, Cx43, Cx45, and Cx30.2) revealed that the *Gja1* promoter contains an evolutionarily conserved element harboring a putative Irx3 binding site (37–39), which overlaps with an Nkx2-5 binding motif (Irx/NKE) immediately upstream of conserved T-box binding elements (Fig. 4*E*). The conserved element is 198 bp in size and is located at genomic coordinates (mm9) chr10:56,096,566–56,096,763. To determine whether Irx3 binds the *Gja1* promoter in vivo, we performed chromatin immunoprecipitation with ventricles isolated from the $Irx3^{3myc\text{-}6his}$ knock-in mouse line, which express C-terminally tagged Irx3 protein under endogenous gene expression control (Fig. S1 *B* and *C*). Enrichment for $Irx3^{3myc\text{-}6his}$ was detected at the *Gja1* promoter region containing the Irx/NKE element and the core *Gja1* promoter, but not at an intergenic region or at the *Nppa* promoter (Fig. 4*F*). Moreover, coimmunoprecipitation shows that Irx3 can form a protein complex with Nkx2-5 (Fig. 4*G*). We then examined whether Irx3 and Nkx2-5 could regulate *Gja1* transcription in vitro and found that Irx3 indeed antagonizes Nkx2-5-dependent activation of a *Gja1–luciferase* reporter containing 1.68 kb of the endogenous promoter sequence (40) in transfected COS7 cells (Fig. 4*H*). Furthermore, three point mutations, made to alter predicted core binding sequences recognized by Irx3, diminished the ability of Irx3 to exert repression of *Gja1–luciferase* in the presence of increasing amounts of Nkx2-5. In the proximal VCS, where these transcription factors at expressed at high levels, Irx3 could therefore repress Nkx2-5-mediated activation of *Gja1* transcription. Furthermore, direct binding of Irx3 to the *Gja1* promoter may lead to transcriptional repression through its interactions with Nkx2-5 or Tbx5 and/or through recruitment of corepressors through a mechanism similar to that of Irx5 (13).

In this study, we demonstrate that Irx3 is a unique transcriptional regulator of rapid electrical conduction that is necessary to drive ventricular activation. To address whether *Irx3* function is evolutionarily conserved, we examined its role in zebrafish, where the *ziro3a* ortholog is expressed in the heart at 48 h after fertilization (Fig. S7 *A* and *B*). Optical mapping was performed in live zebrafish expressing the in vivo calcium transient reporter *Tg*(*cmlc2*:*gCaMP*)^{s878} (41). Similar to our observations in mice, inhibition of *ziro3a* by morpholino antisense oligonucleotides caused slowed and abnormal impulse conduction in the ventricle (Fig. S7*C*).

Concluding Remarks

The *Irx* gene family of transcription factors has evolutionarily conserved roles during embryonic development (10) and is expressed in the developing mouse heart. We have shown that *Irx5* represses transcription of the voltage-gated potassium channel gene *Kv4.2* to establish an epicardial-to-endocardial repolarization gradient (12–16). Our present study identifies a previously undescribed role for an additional *Iroquois* factor, *Irx3*, in the tight regulation of gap junction gene expression in specialized His–Purkinje system cells, where its expression is highly enriched. Irx3 regulation of Cx expression is likely to be relevant to the electrical maturation of other excitable cell types, such as those of the central nervous system enriched in Irx3 expression (14, 42).

Our studies reveal an important role of Irx3 in the precise transcriptional control of intercellular coupling and synchronized ventricular depolarization. Interestingly, the electrical phenotypes in mice lacking Irx3 are commonly associated with inherited

increased risk of arrhythmias and heart failure (2). Furthermore, it has been shown that defects in cardiac impulse conduction can directly lead to aberrant cardiac remodeling and reduced cardiac function (43). Thus, it may be informative to determine whether deleterious mutations reside in the human *IRX3* gene.

Materials and Methods

Details of materials and methods are provided in *SI Materials and Methods*. All animal work was conducted according to the regulations provided by the Animal Care and Use Committees. β-Galactosidase and Masson's trichrome staining of fixed embryos and tissue (4% paraformaldehyde) was carried out by using standard methods. Optical projection tomography (OPT) imaging of hearts was performed as described (44). Fluorescence in situ hybridization in zebrafish was performed as described (41). For immunofluorescence detection, four-chambered view serial cryosections (8 μm) were stained with various antisera as described in *SI Materials and Methods*. Transthoracic echocardiography was used for noninvasive serial assessment of cardiac function in mice as described (13, 45). Surface ECG (leads I and II) was obtained at P12 and at 8–10 wk as described (13). For Cx protein imaging, the Scan Large Image function of NIS Elements was used to stitch high-resolution (60×/1.49 Apo TIRF objective) widefield epifluorescence images encompassing the entire septum. Differences between groups were examined for statistical significance by using the Student *t* test. $P < 0.05$ was regarded as significant.

ACKNOWLEDGMENTS. We thank V. Vedantham for initial help with FACS; B. Black for Mef2AHF::Cre mice, D. Zhao, W. Yang, B. M. Steer, and M. Chalsev for technical support; the Gladstone Flow Cytometry and Histology Cores for technical support; and G. Howard for editorial assistance. *Irx3::EGFP* BAC transgenic mice were obtained from the Gene Expression Nervous System Atlas (GENSAT) Project (National Institute of Neurological Disorders and Stroke Contracts N01NS02331 and HHSN271200723701C to The Rockefeller University). S.-S.Z. was funded by the Heart and Stroke Foundation of Canada. S.-S.Z. and N.G. are funded by American Heart Association studentships and fellowships, respectively. J.W.S. was funded by the American Federation for Aging Research and by American Heart Association Grant SDG3420042. K.-H.K and A.R. were supported by the Ontario Graduate Scholarship in Science and Technology and the Heart & Stroke Richard Lewar Centre of Excellence. A.R. was supported by a Heart and Stroke Foundation of Canada master's studentship. This work was funded by Canadian Institutes of Health Research grants (to C.-c.H. and P.H.B.); National Institutes of Health (NIH)/National Heart, Lung, and Blood Institute Grants R01 HL93414 ARRA (to B.G.B.) and R01 HL94414 (to R.M.S.); the Lawrence J. and Florence A. DeGeorge Charitable Trust/American Heart Association Established Investigator Award (to B.G.B.); NIH/National Center for Research Resources Grant C06 RR018928 (to the J. David Gladstone Institutes); and William H. Younger, Jr. (B.G.B.).

1. Cohen SI, Lau SH, Stein E, Young MW, Damato AN (1968) Variations of aberrant ventricular conduction in man: Evidence of isolated and combined block within the specialized conduction system. An electrocardiographic and vectorcardiographic study. *Circulation* 38:899–916.
2. Iuliano S, Fisher SG, Karasik PE, Fletcher RD, Singh SN; Department of Veterans Affairs Survival Trial of Antiarrhythmic Therapy in Congestive Heart Failure (2002) QRS duration and mortality in patients with congestive heart failure. *Am Heart J* 143: 1085–1091.
3. Rudy Y, Shaw RM (1997) Cardiac excitation: An interactive process of ion channels and gap junctions. *Adv Exp Med Biol* 430:269–279.
4. Moskowitz IP, et al. (2007) A molecular pathway including Id2, Tbx5, and Nkx2-5 required for cardiac conduction system development. *Cell* 129:1365–1376.
5. Bakker ML, et al. (2008) Transcription factor Tbx3 is required for the specification of the atrioventricular conduction system. *Circ Res* 102:1340–1349.
6. Meysen S, et al. (2007) Nkx2.5 cell-autonomous gene function is required for the postnatal formation of the peripheral ventricular conduction system. *Dev Biol* 303: 740–753.
7. Rentschler S, et al. (2002) Neuregulin-1 promotes formation of the murine cardiac conduction system. *Proc Natl Acad Sci USA* 99:10464–10469.
8. Hyer J, et al. (1999) Induction of Purkinje fiber differentiation by coronary arterialization. *Proc Natl Acad Sci USA* 96:13214–13218.
9. Hall CE, et al. (2004) Hemodynamic-dependent patterning of endothelin converting enzyme 1 expression and differentiation of impulse-conducting Purkinje fibers in the embryonic heart. *Development* 131:581–592.
10. Gómez-Skarmeta JL, Modolell J (2002) Iroquois genes: Genomic organization and function in vertebrate neural development. *Curr Opin Genet Dev* 12:403–408.
11. Matsumoto K, et al. (2004) The prepattern transcription factor Irx2, a target of the FGF8/MAP kinase cascade, is involved in cerebellum formation. *Nat Neurosci* 7: 605–612.
12. Bruneau BG, et al. (2001) Cardiomyopathy in Irx4-deficient mice is preceded by abnormal ventricular gene expression. *Mol Cell Biol* 21:1730–1736.
13. Costantini DL, et al. (2005) The homeodomain transcription factor Irx5 establishes the mouse cardiac ventricular repolarization gradient. *Cell* 123:347–358.
14. Cohen DR, Cheng CW, Cheng SH, Hui CC (2000) Expression of two novel mouse Iroquois homeobox genes during neurogenesis. *Mech Dev* 91:317–321.
15. Mummenhoff J, Houweling AC, Peters T, Christoffels VM, Rüther U (2001) Expression of Irx6 during mouse morphogenesis. *Mech Dev* 103:193–195.
16. Christoffels VM, Keijser AG, Houweling AC, Clout DE, Moorman AF (2000) Patterning the embryonic heart: identification of five mouse Iroquois homeobox genes in the developing heart. *Dev Biol* 224:263–274.
17. Callahan CA, Thomas JB (1994) Tau-beta-galactosidase, an axon-targeted fusion protein. *Proc Natl Acad Sci USA* 91:5972–5976.
18. Virágh S, Challice CE (1982) The development of the conduction system in the mouse embryo heart. *Dev Biol* 89:25–40.
19. Miquerol L, et al. (2004) Architectural and functional asymmetry of the His-Purkinje system of the murine heart. *Cardiovasc Res* 63:77–86.
20. Verzi MP, McCulley DJ, De Val S, Dodou E, Black BL (2005) The right ventricle, outflow tract, and ventricular septum comprise a restricted expression domain within the secondary/anterior heart field. *Dev Biol* 287:134–145.
21. Danielian PS, Muccino D, Rowitch DH, Michael SK, McMahon AP (1998) Modification of gene activity in mouse embryos in utero by a tamoxifen-inducible form of Cre recombinase. *Curr Biol* 8:1323–1326.
22. Delorme B, et al. (1997) Expression pattern of connexin gene products at the early developmental stages of the mouse cardiovascular system. *Circ Res* 81:423–437.
23. Castellanos A, Jr., Maytin O, Arcebal AG, Lemberg L (1970) Significance of complete right bundle-branch block with right axis deviation in absence of right ventricular hypertrophy. *Br Heart J* 32:85–92.
24. Nygren A, et al. (2000) Voltage-sensitive dye mapping of activation and conduction in adult mouse hearts. *Ann Biomed Eng* 28:958–967.
25. Fast VG, Kléber AG (1995) Block of impulse propagation at an abrupt tissue expansion: evaluation of the critical strand diameter in 2- and 3-dimensional computer models. *Cardiovasc Res* 30:449–459.
26. Fast VG, Kléber AG (1995) Cardiac tissue geometry as a determinant of unidirectional conduction block: Assessment of microscopic excitation spread by optical mapping in patterned cell cultures and in a computer model. *Cardiovasc Res* 29: 697–707.
27. Myerburg RJ (1971) The gating mechanism in the distal atrioventricular conducting system. *Circulation* 43:955–960.
28. Gourdie RG, et al. (1993) The spatial distribution and relative abundance of gap-junctional connexin40 and connexin43 correlate to functional properties of components of the cardiac atrioventricular conduction system. *J Cell Sci* 105:985–991.
29. Bevilacqua LM, et al. (2000) A targeted disruption in connexin40 leads to distinct atrioventricular conduction defects. *J Interv Card Electrophysiol* 4:459–467.
30. Kirchhoff S, et al. (1998) Reduced cardiac conduction velocity and predisposition to arrhythmias in connexin40-deficient mice. *Curr Biol* 8:299–302.
31. Simon AM, Goodenough DA, Paul DL (1998) Mice lacking connexin40 have cardiac conduction abnormalities characteristic of atrioventricular block and bundle branch block. *Curr Biol* 8:295–298.
32. Rackauska s M, et al. (2007) Gating properties of heterotypic gap junction channels formed of connexins 40, 43, and 45. *Biophys J* 92:1952–1965.
33. Lisewski U, et al. (2008) The tight junction protein CAR regulates cardiac conduction and cell-cell communication. *J Exp Med* 205:2369–2379.
34. Cottrell GT, Burt JM (2001) Heterotypic gap junction channel formation between heteromeric and homomeric Cx40 and Cx43 connexons. *Am J Physiol Cell Physiol* 281: C1559–C1567.
35. Cottrell GT, Burt JM (2005) Functional consequences of heterogeneous gap junction channel formation and its influence in health and disease. *Biochim Biophys Acta* 1711: 126–141.
36. Valiunas V, Gemel J, Brink PR, Beyer EC (2001) Gap junction channels formed by coexpressed connexin40 and connexin43. *Am J Physiol Heart Circ Physiol* 281:H1675–H1689.
37. Berger MF, et al. (2008) Variation in homeodomain DNA binding revealed by high-resolution analysis of sequence preferences. *Cell* 133:1266–1276.
38. Noyes MB, et al. (2008) Analysis of homeodomain specificities allows the family-wide prediction of preferred recognition sites. *Cell* 133:1277–1289.
39. Bilioni A, Craig G, Hill C, McNeill H (2005) Iroquois transcription factors recognize a unique motif to mediate transcriptional repression in vivo. *Proc Natl Acad Sci USA* 102:14671–14676.
40. Chen ZQ, et al. (1995) Identification of two regulatory elements within the promoter region of the mouse connexin 43 gene. *J Biol Chem* 270:3863–3868.
41. Chi NC, et al. (2008) Genetic and physiologic dissection of the vertebrate cardiac conduction system. *PLoS Biol* 6:e109.
42. Kobayashi D, et al. (2002) Early subdivisions in the neural plate define distinct competence for inductive signals. *Development* 129:83–93.
43. Chi NC, et al. (2010) Cardiac conduction is required to preserve cardiac chamber morphology. *Proc Natl Acad Sci USA* 107:14662–14667.
44. Sharpe J, et al. (2002) Optical projection tomography as a tool for 3D microscopy and gene expression studies. *Science* 296:541–545.
45. Zhou YQ, et al. (2004) Comprehensive transthoracic cardiac imaging in mice using ultrasound biomicroscopy with anatomical confirmation by magnetic resonance imaging. *Physiol Genomics* 18:232–244.

Supporting Information

Zhang et al. 10.1073/pnas.1106911108

SI Materials and Methods

Gene Targeting and Mice. A loss-of-function mutation in *Irx3* was generated in R1 embryonic stem (ES) cells by replacing part of exon 1 with a *tauLacZ* reporter after the start codon. Generation of $Irx3^{3myc\text{-}6his}$ mice was achieved by inserting three myc-tags (EQKLISEEDL) and six histidines at the C terminus of Irx3. ES cell lines with the desired mutation were identified by Southern analysis and germ-line transmission was achieved by standard procedures. PCR genotyping of $Irx3^{tauLacZ}$ was carried out using these primers: GAGTTGGCCGCCTCTGGGTCCCTATCCAAT, CCCTCTCTCCCGGGTTTCTCTGGCTCTTAC, and GAATTCGCCAATGACAAGACGCTGGGCGGG.

Genotyping of $Irx3^{3myc6his}$ mice was carried out using these primers: CAAGAAGGGGTGATGAGAGTCGCTGGGCG and GGAGAGGGAACCACGGCGAGAAAGGCCTA. $Irx3^{tauLacZ}$ mice were crossed with $Cx40^{EGFP}$ to generate mice for GFP and LacZ colocalization experiments. *ROSA-YFP;* $Irx3^{tauLacZ/+}$ mice were crossed with either *Mef2CAHF::Cre* or *Wnt1-Cre* mice for lineage analysis. All analysis was done in the *C57BL/6* background. Animals were cared for in accordance with national and institutional requirements.

Expression Analysis. β-Galactosidase and Masson's trichrome staining of fixed embryos and tissue [4% paraformaldehyde (PFA)] was carried out using standard methods. Whole-mount visualization of the conduction fibers was achieved in postfixed hearts cleared by 1:2 benzyl alcohol to benzyl benzoate (BABB). Optical projection tomography (OPT) imaging of hearts was performed as described (1). Fluorescence in situ hybridization in zebrafish was performed as described (2). For immunofluorescence detection, 4-chambered view serial cryo sections (8-μm) were stained with primary antibodies against Hcn4 (Alome Labs), LacZ (Cappel), Cx40 (Chemicon), GFP (Abcam), Cx43 (Sigma), tropomyosin (Hybridoma Bank), PECAM (Hybridoma Bank), Scn5a (Alome Labs), and *N*-cadherin (BD Biosciences). Secondary detection was carried out using Alexa488-, Alexa555-, and Alexa 647-conjugated antibodies (Invitrogen). Nuclei detection and mounting were achieved using ProLong Immuno-Gold reagent containing DAPI (Invitrogen).

Myocyte Isolation and Cell Assays. Hearts were harvested and digested with 0.25 mg/mL trypsin (Invitrogen) and 50 U/mL type II collagenase (Worthington) in calcium- and bicarbonate-free Hanks' buffer with Hepes (HBSS) at 37 °C, as described (3). Cells from either wild-type or Irx3-null mice, each expressing the *Irx3::EGFP* reporter, were isolated from the proximal VCS. Cell pairs were analyzed for clear Cx plaque expression at cell borders and quantified. For calcium flux assays, medium was replaced with HBSS containing 2% serum, and GFP^+ cells were identified by widefield epifluorescence. Cells were incubated with Fluo-4:00 AM (5mM, Invitrogen) for 15 min before acquisition. Images were acquired at a rate of 100 fps using a Nikon Eclipse *Ti* microscope with 20×/0.75 Plan Apo objective and Cascade II 512 camera controlled by NIS elements software.

Laser Capture Microdissection. GFP-positive VCS cells from frozen sections were visualized and captured onto a CapSure Macro LCM cap (Molecular Devices, Sunnyvale, CA) with a PixCell II System equipped with epifluorescence optics (Arcturus, Mountain View, CA), a spot size of 7.5 μm, power of 60–80 mV, and pulse duration of 700 μs . Subendocardial and subepicardial cells were also captured on separate caps. RNA was isolated using the Arcturus Pico Pure RNA isolation kit.

Heart Function Measurements. Transthoracic echocardiography was used for noninvasive serial assessment of cardiac function in mice with a Vevo 770 μLtrasound machine (VisualSonics) as described (3, 4). Surface ECG (lead I and II) was obtained at P12 and at 8–10 wk as described (3). For telemetry ECG, telemetry devices (Data Sciences International; St. Paul, MN) were implanted dorsally with electrodes in lead II configuration. Mice were allowed to recover for 60 h postsurgery before ECG data were collected and analyzed. Intracardiac ECG was measured in anesthetized mice (1.5% isoflurane) while body temperature was maintained around 36.8 ± 0.3 °C, using a 2-French octapolar electrode catheter (CIBer mouse EP catheter; NuMed, Hopkinton, NY) as described (3).

Optical Mapping and Analysis. Activation mapping in zebrafish was performed as described (2). Cannulated hearts were perfused with 37 °C Krebs solution (pH 7.4) at a constant flow rate of 3.5 mL/min for a 15-min equilibration period, followed by 10-min perfusion of voltage-sensitive dye, di-4-ANEPPS. Hearts were excited using an EXFO X-Cite exact source filtered at 543 ± 11 nm, and high-resolution optical images were taken using an upright Olympus MVX-10 microscope equipped with a Photometric Cascade 128+ CCD camera interfaced with ImagePro Plus 5.1 software. Resolution of image sequences captured was 16-bit, 63 × 64 pixel at 923Hz. While the hearts were perfused with a modified Krebs–Henseleit solution containing 0.3 mM Ca^{2+} at room temperature, action potentials (AP) were gathered using two fine-tip glass electrodes (A-M Systems model 3100) on the Purkinje fibers identified by *Cx40* promoter-driven EGFP. Conduction velocity was calculated by the time interval between peaks of two APs divided by the distance between the electrodes.

Connexin Imaging and Quantitation. The Scan Large Image function of NIS Elements was used to stitch high-resolution (60×/1.49 Apo TIRF objective) widefield epifluorescence images encompassing the entire septum. With the ImageJ software, GFP images were converted to binary masks. Within this mask image, GFP^+ regions had a value = 1, and all remaining pixels had a value = 0. Masks were image-multiplied by corresponding Cx40 or Cx43 images to exclude all signals except that from GFP^+ cells, and fluorescence intensity was subsequently measured. To account for slide-to-slide variance, two random 400 × 400 pixel regions of interest were measured in GFP^- regions of the septum. Similarly, background was determined for each image with a 400 × 400 pixel tissue-free region of interest and subtracted from all values. Fluorescence intensity in the proximal VCS was then normalized to that of the septal working myocardium, and graphs were plotted using Prism 5 software (Graphpad).

Dye Injection. Cardiac slices were prepared from freshly isolated hearts as described (5). Live 250-μm-thick slices were obtained in central 4-chambered view to expose proximal right bundle branches along the septum. Glass micropipettes (Femtotips II; Eppendorf) were loaded with 5 mM AexaFluor594 hydrazide sodium salt (Invitrogen) in 200 mM KCl. Individual $Irx3::EGFP^+$ cells were microinjected at 50 hPa pressure for 0.2 s with a FemtoJet apparatus (Eppendorf) and micromanipulator. Four minutes post injection, sections were fixed in 4% PFA overnight at 4 °C. Z-stacks of mounted sections were acquired by spinning

disk confocal microscopy with a Nikon T*i* microscope with a 20×/0.75 Plan Apo objective, Yokogowa CSU-X1 spinning disk confocal unit with 561- and 647-nm DPSS laser sources and a Coolsnap HQ^2 camera controlled by NIS Elements software. The Nikon Eclipse *Ti* microscope had a 20×/075 plan Apo objective, and the Coolsnap HQ^2 camera was controlled by NIS elements software. Maximum intensity projections of 25-μm Z-stacks (0.5-μm intervals) were generated, and dye penetration was measured using ImageJ software (NIH).

In Vitro Gene Expression. Transfections and Luciferase assays were performed as described (3). Adenoviral Irx3 constructs were generated using Adeno-X ViraTrak Expression System 2 (Clontech). NVMs were infected for 3–4 h with adenovirus at a multiplicity of infection (MOI) of 5 and cultured in fresh serum medium.

Coimmunoprecipitation and Immunoblotting. Coimmunoprecipitation was performed in COS-7 cells as described (3). Cell lysates were incubated with the indicated antibodies overnight at 4 °C; immunoprecipitates were pulled down with protein G–Sepharose beads and immunoblotted with the indicated antibodies overnight at 4 °C, following standard protocols.

Chromatin Immunoprecipitation. Chromatin was isolated from hearts expressing $Irx3^{3myc6his}$. The Imprint Chromatin Immunoprecipitation Kit (Sigma) was used according to the manufacturer's instructions to capture Myc-tagged Irx3 protein. DNA fragments were analyzed by custom Taqman assays.

Nppa proximal promoter: 5′-GGGACCACCACATATTTC-ATGCT-3′, and 5′-GTGTCCAAGGTGCCAACAG-3′. For intergenic *Gja1*: 5′-GGACAGACATCTGCCAAGGT-3′, and 5′-ATGCCCCTCAGCTATCACAC-3′. For *Gja1* core promoter: 5′-GCCCCTCCTTCCAGTTGAG-3′, and 5′-TTTTTAACTT-GGAGCACAGAGCTTT-3′. For the conserved binding site: 5′-GGTCTGGTTGTGAAATGCCTTT-3′, and R 5′-CTCTTC-CTCTTAAACCCGGACAATT-3′.

Quantitative PCR. Total RNA was isolated with TRIzol reagent (Invitrogen), and cDNA was synthesized with SuperScript II reverse transcriptase (Invitrogen). Primers for mouse *Irx3*, *Gja5*, *Gja1*, and *GAPDH* are as follows: *Irx3* forward, 5′-GGCCGC-CTCTGGGTCCCTAT-3′; reverse, 5′-GAGCGCCCAGCTGT-GGGAAG-3′; *Gja5* forward, 5′-AAGCAGAAGGCTCGGCC-TC-3′; reverse, 5′-GGAAGCTCCAGTCACCCATCTT-3′; *Gja1* forward, 5′-TCATTAAGTGAAAGAGAGGTGCCC-3′; reverse, 5′-TGGAGTAGGCTTGGACCTTGTC-3′; GAPDH, TaqMan Rodent GAPDH Control Reagents.

FACS. FACS sorting of single cells isolated from $Irx3::EGFP^{+}$ ventricles was carried out using FACSDiva and FlowJo.

Statistical Analysis. Differences between groups were examined for statistical significance by using the Student *t* test. *P* values of <0.05 were regarded as significant.

1. Sharpe J, et al. (2002) Optical projection tomography as a tool for 3D microscopy and gene expression studies. *Science* 296:541–545.
2. Chi NC, et al. (2008) Genetic and physiologic dissection of the vertebrate cardiac conduction system. *PLoS Biol* 6:e109.
3. Costantini DL, et al. (2005) The homeodomain transcription factor Irx5 establishes the mouse cardiac ventricular repolarization gradient. *Cell* 123:347–358.
4. Zhou YQ, et al. (2004) Comprehensive transthoracic cardiac imaging in mice using ultrasound biomicroscopy with anatomical confirmation by magnetic resonance imaging. *Physiol Genomics* 18:232–244.
5. Rackauskas M, et al. (2007) Gating properties of heterotypic gap junction channels formed of connexins 40, 43, and 45. *Biophys J* 92:1952–1965.

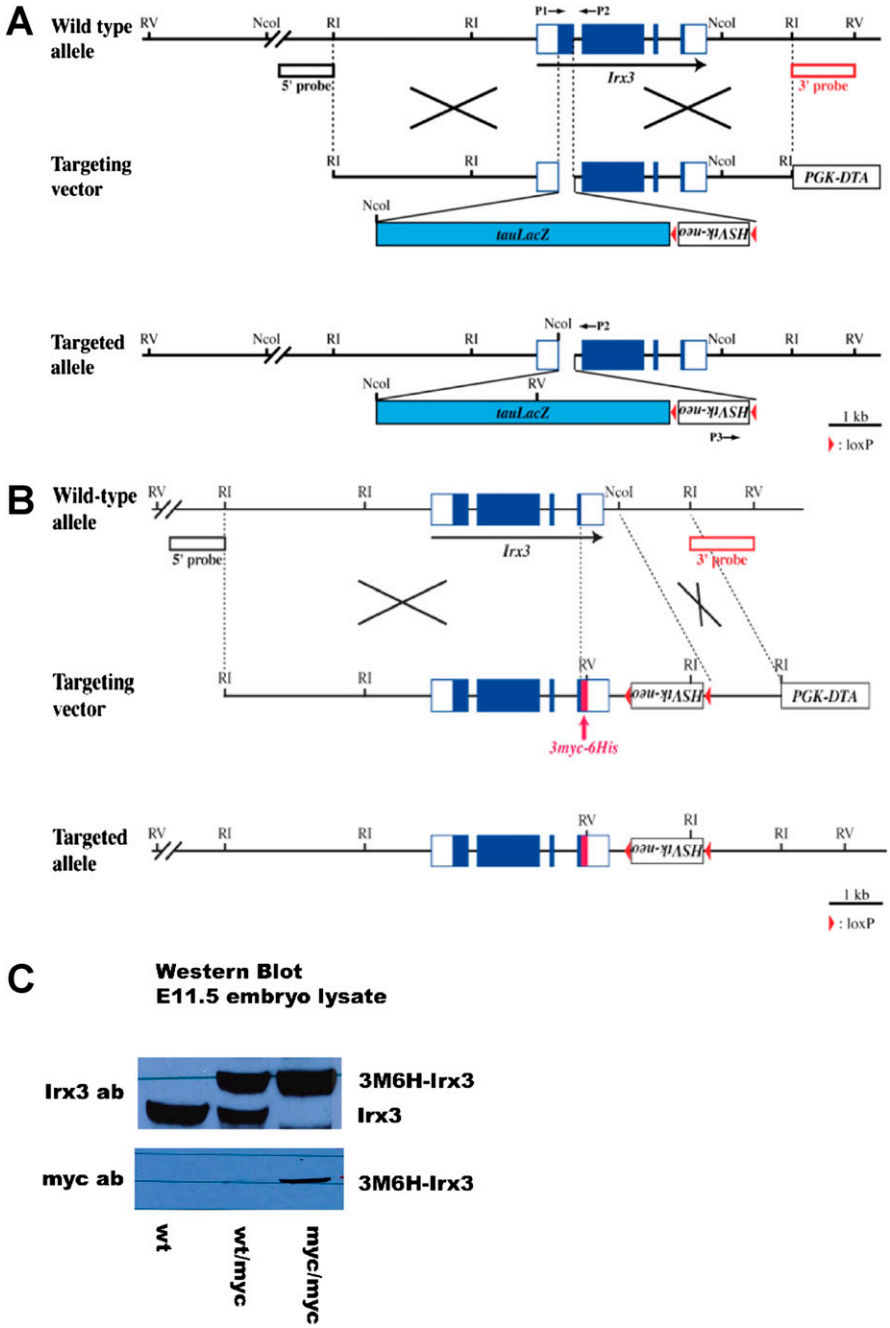

Fig. S1. Gene targeting strategies of *Irx3*^{tauLacZ} and *Irx3*$^{3myc\text{-}6his}$ mice. (*A*) A loss-of-function mutation in Irx3 was made in ES cells by replacing part of exon 1 with a *tauLacZ* reporter immediately after the start codon. (*B*) Generation of *Irx3*$^{3myc\text{-}6his}$ mice was achieved by inserting three myc tags and six histidines at the C terminus. (*C*) Irx3$^{3myc\text{-}6his}$ protein was detected in whole embryo lysates using antibodies against Irx3 and myc tag.

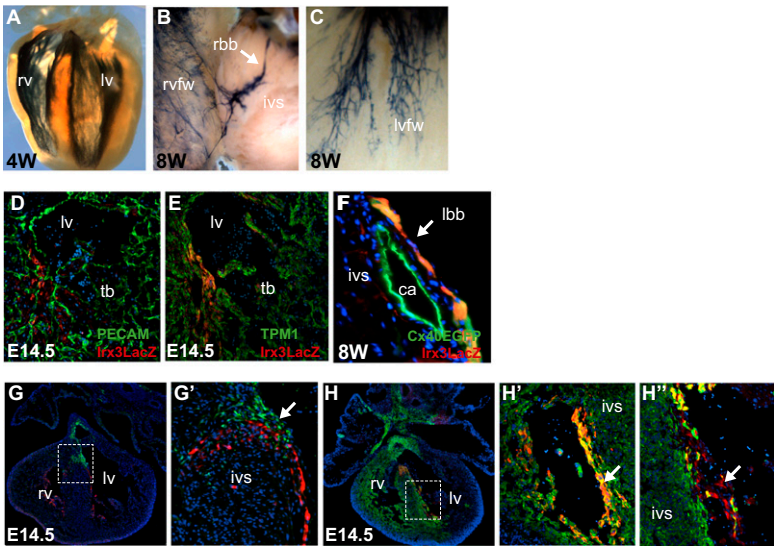

Fig. S2. *Irx3*^{tauLacZ} is highly expressed in the VCS. Irx3^{+} subendocardial myocytes preferentially express Cx40 at cell borders. (*A*) Whole-mount *LacZ* staining shows that *Irx3*^{tauLacZ} is expressed in the His–Purkinje system at 4 wk. (*B*) An *Irx3*$^{LacZ+}$ right bundle branch is shown extending along the septum toward the right ventricular free wall (rvfw). (*C*) *Irx3*$^{tauLacZ+}$ Purkinje fibers along the left ventricular free wall (lvfw) are shown. (*D*) *Irx3*^{tauLacZ} (red) colocalizes with myocyte-specific tropomyosin (TMP1, green) at E14.5. (*E*) *Irx3*$^{tauLacZ+}$ (red) trabeculae (tb) are surrounded by PECAM+ (green) cells of the developing endocardium. (*F*) Colocalization of *Irx3*^{tauLacZ} with Cx40EGFP in the adult VCS but not in coronary arteries (ca). (*G* and *G*′) Lineage analysis in mice expressing *Irx3*^{tauLacZ} (red) and *Wnt1-Cre*/ROSA-YFP (green) show that Cre-labeled neural crest-derived cells are closely associate with the VCS, but do not make direct contributions to the conduction tissue. (*H*, *H*′, and *H*″) *Irx3*$^{tauLacZ+}$ VCS cells (red) are predominantly derived from the *Mef2CAHF::Cre*/ROSA-YFP-labeled ventricular myocyte lineage, with the exception of *Irx3*$^{tauLacZ+}$ cells of the developing distal VCS in the left ventricle (arrows).

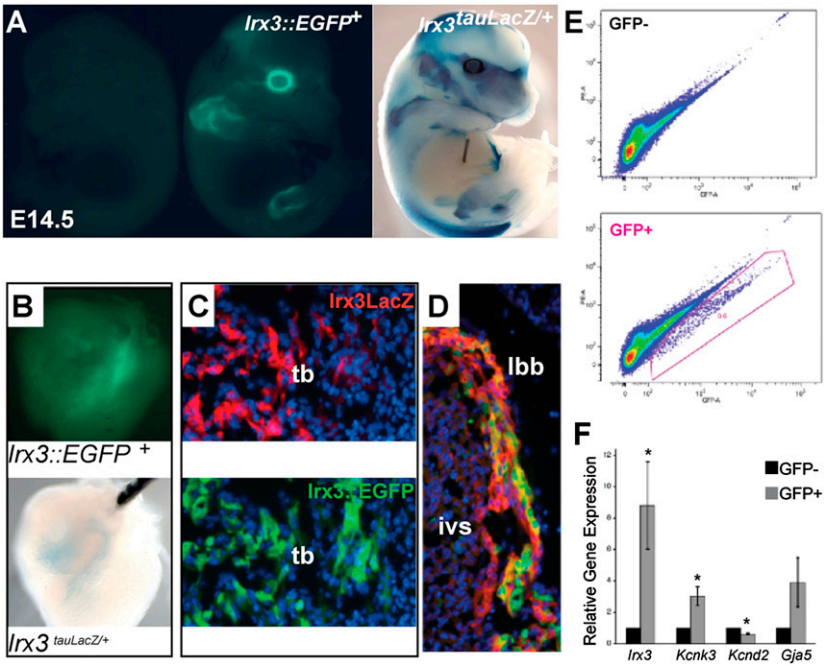

Fig. S3. Characterization of the *Irx3::EGFP* BAC allele shows that it is coexpressed with VCS markers. (*A*) Comparison of whole embryo expression of the *Irx3::EGFP* and *Irx3*^{LacZ} reporters reveal their similar expression patterns in the brain, eyes, and limbs at E14.5. (*B*) Both reporters are found in the developing heart. (*C* and *D*) Immunofluorescence detection of *LacZ* (red) and GFP (green) in mice that express both reporters confirms their colocalization in the developing VCS. (*E*) FACS sorting was used to obtain live *Irx3::EGFP*$^{+}$ cells. (*F*) Sorted *Irx3::EGFP*+ cells are enriched in VCS markers such as Kcnk3, Kcnd2, and Gja5 (normalized by GAPDH). $n = 4$; $^{*}P < 0.05$ vs. GFP-negative population. tb, trabeculae; ivs, interventricular septum; lbb, left bundle branch.

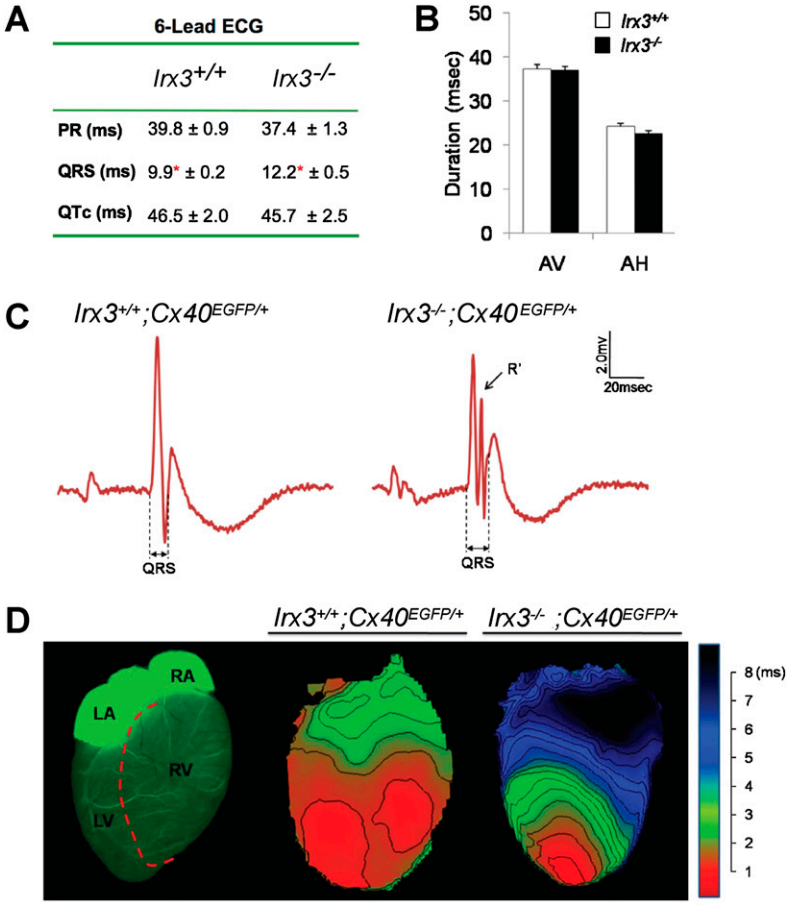

Fig. S4. Surface ECG and optical mapping shows delayed and asynchronous ventricular activation in *Irx3*-null mice. (*A*) Summary of surface ECG results showing PR, QRS, and QTc intervals in adult mice. (*B*) Consistent with the absence of Irx3 expression in the atria or AV node, A-V and H-V conduction times are unchanged in *Irx3*-null mice. (*C*) QRS prolongation and notched R waves were observed in ex vivo perfused hearts lacking Irx3. (*D*) Mice heterozygous for Cx40 show normal ventricular activation with two breakthrough points. Compound Irx3 and Cx40 mutants display abnormal ventricular activation.

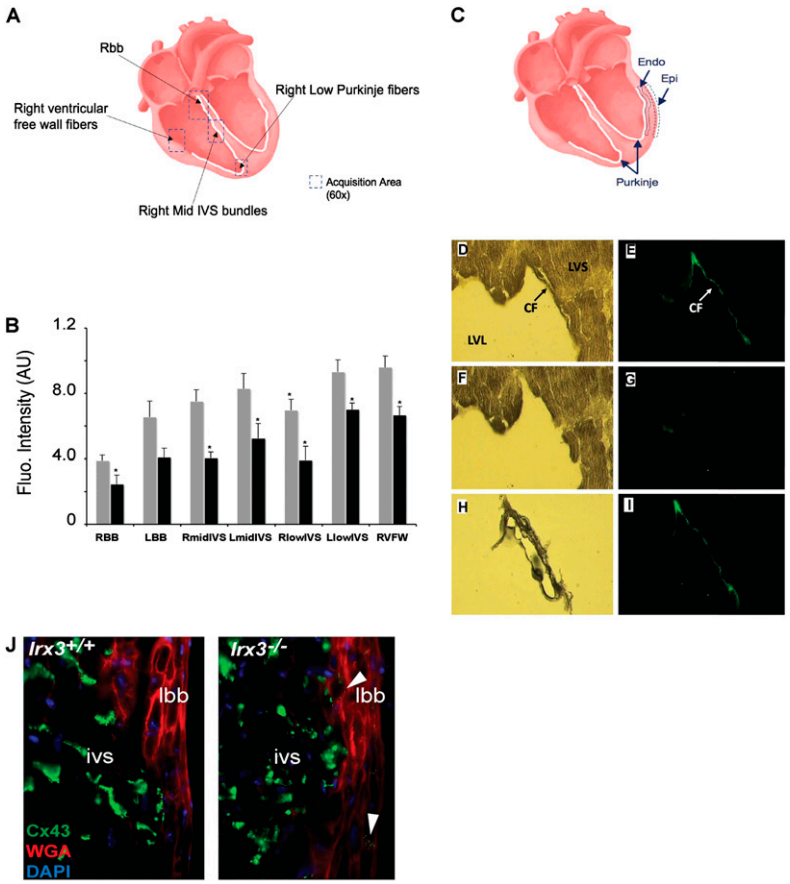

Fig. S5. Laser capture microdissection of VCS cells. (*A*) Diagram depiction of where images were acquired for Cx40 plaque intensity analysis. (*B*) Quantitation of fluorescence intensity in the areas indicated, measured for both sides of the heart, shows a decrease in Cx40 plaque expression in adult hearts lacking Irx3. (*C*) Diagram depiction of where cells were isolated for LCM. (*D* and *E*) Before laser capture. (*F* and *G*) Following laser capture of conduction fiber. (*H* and *I*) Isolated conduction fiber located on the LCM capsule. (*J*) Cx43 immunolabeling reveals ectopic protein plaque expression in the proximal LBBs (marked by high WGA expression, red) of adult hearts lacking Irx3. LVL, left ventricular lumen; LVS, left ventricular septum; CF, conduction fiber; RmidIVS, right midportion of the IVS; RlowIVS, right lower portion of the IVS; WGA, wheat germ agglutinin.

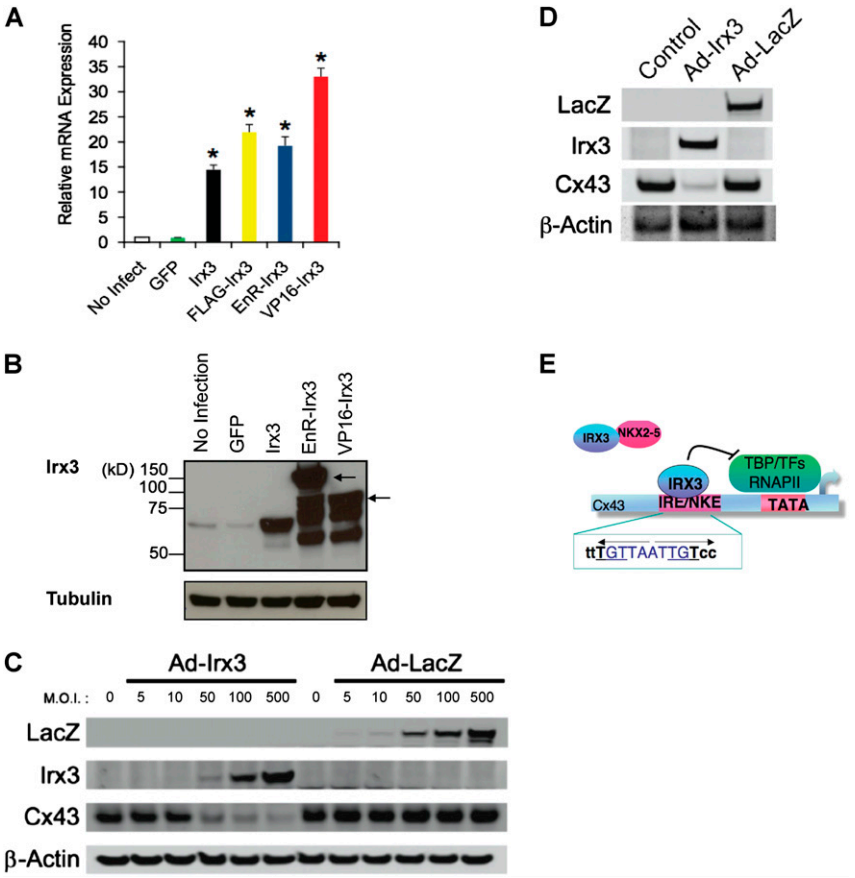

Fig. S6. Irx3 regulation of Gja1 and Gja5 expression. (*A*) Irx3 mRNA was expressed at similar levels in NVMs infected with adenoviruses carrying the various overexpression constructs.*, $P < 0.01$. (*B*) Western blot shows Irx3 protein overexpression was achieved in infected cells. (*C*) Irx3 overexpression in HeLa cells led to Cx43 repression in a dose-dependent manner. (*D*) Adenoviral infection of NVMs at MOI of 5 resulted in marked decrease of Cx43 protein. (*E*) A model for Gja1 transcriptional repression by Irx3.

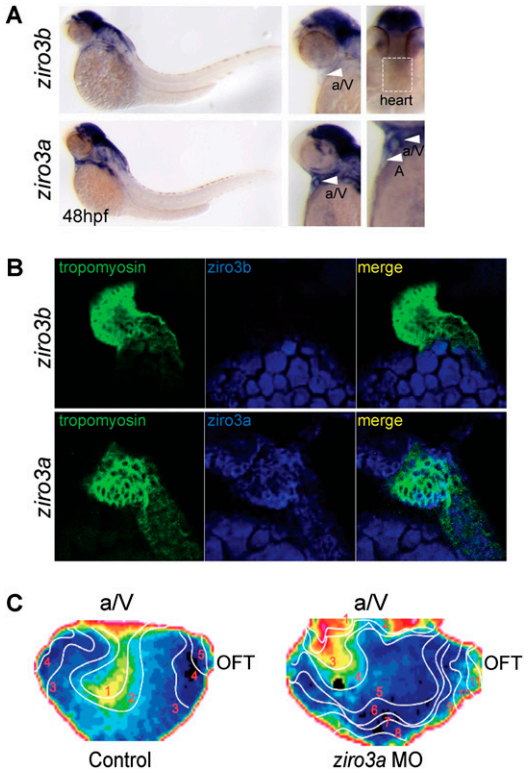

Fig. S7. Ziro3a is required for ventricular activation in zebrafish. (*A*) The Irx3 ortholog ziro3a, but not the more divergent ziro3b, is expressed in the heart at 48 h after fertilization. (*B*) Fluorescence in situ hybridization shows strong colocalization of ziro3a and myocyte-specific tropomyosin-1 in the ventricle. (*C*) Optical mapping of live zebrafish expressing the Tg (cmlc2:gCaMP)-s878 calcium reporter shows that inhibition of ziro3a by morpholino oligonucleotides-tides caused abnormal impulse conduction in the ventricle. Each isochronal line represents 40 ms. A, atria; V, ventricle; a/V, atrioventricular canal; OFT, outflow tract; MO, morpholino knockdown.

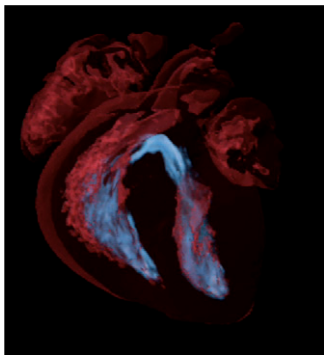

Movie S1. Optical projection tomography reconstruction of an E16.5 heart. Blue signal is *Irx3*^{LacZ}; red signal is myocardial tissue.

Movie S1

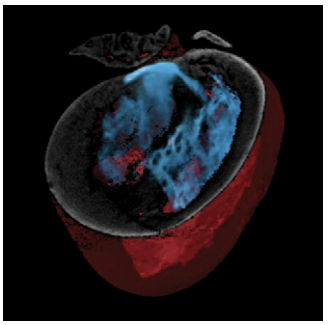

Movie S2. Optical projection tomography reconstruction of a postnatal day 3 heart. Blue signal is *Irx3*^{LacZ}; red signal is myocardial tissue.

Movie S2

Other Supporting Information Files

Dataset S1 (XLS)